

Efficient Reduction of CO₂ to Formate Using in Situ Prepared Nano-Sized Bi Electrocatalyst

Jingjing Bei¹, Rui Zhang^{2,*}, Zhidong Chen¹, Weixin Lv², Wei Wang^{2,*}

¹ School of Petrochemical Engineering, Changzhou University, Changzhou 213164, P. R. China

² School of Chemistry and Chemical Engineering, Yancheng Institute of Technology, Yancheng 224051, P. R. China

*E-mail: zhangrui20128@163.com, wangw@ycit.edu.cn

Received: 3 January 2017 / Accepted: 31 January 2017 / Published: 12 February 2017

Carbon dioxide (CO₂) can be reduced to valuable chemicals under the suitable cathode potential. During the electrochemical reduction of CO₂, most metal oxide catalysts will be reduced to zero valent metals. In this work, flower-like Bi₂O₃ precursor has been prepared by the method of hydrothermal synthesis, and it has become pure Bi₂O₃ with irregularly shape after calcination at 500 °C for 2 h. The precursor and Bi₂O₃ have been in situ reduced on the glass carbon electrodes separately, then they are used as the electrocatalysts for CO₂ reduction. The faradaic efficiencies for producing formate on the two electrocatalysts are all up to 82% at a low overpotential of 0.89 V. The electrocatalyst reduced from the precursor possesses larger current density for CO₂ reduction than that reduced from Bi₂O₃, and it is believed to be a promising catalyst for further application.

Keywords: Carbon dioxide; Electrochemical reduction; Formate; Metal bismuth; Flower-like

1. INTRODUCTION

In the nature, the CO₂ produced should be balanced with what is consumed to maintain environmental stability. Unfortunately, with the development of human industrial activities, this balance has gradually been disrupted; the concentration of CO₂ in the earth's atmosphere is increasing at an alarming rate in recent years [1]. The application of electrochemical technology to convert CO₂ powered by a renewable electric energy seems a promising approach to reduce the concentration of CO₂ [2-4].

Formate is one of the interesting products from the electrochemical reduction of CO₂ [5]. To realize efficient conversion of CO₂ to formate, much effort has been devoted to the development of high efficient catalysts. Metal complexes [6, 7], pure metals [8, 9], metal oxides [10, 11], polymers

[12] or alloys [13, 14] have been used for the electrochemical reduction of CO₂ to formate. Among them, some metals (such as Hg, Pb, In and Sn) can catalyze the reduction of CO₂ to formate with high selectivity [15]. These studies greatly promoted this area, but most of them showed that the overpotentials for the reduction of CO₂ to formate are too large (>1.0 V) for practical use [8]. Our previously researches reported that the faradaic efficiency for producing formate on Sn-based electrode can reach up to 80% with an overpotential of 1.19 V which is too high and power-wasting [16-20].

Compared with the above metals, metal Bi can reduce CO₂ to formate at lower overpotential. Zhang et al. reported that the faradaic efficiency for producing formate on nano-sized Bi catalyst can achieve to 90% with the overpotential lower than 0.9 V, whereas the faradaic efficiency on the Bi powder (around 38 μm) is lower than 60% [21]. Some researcher also found that the nano-sized metal materials exhibit superior activity in CO₂ reduction compared to the bulk one [22, 23]. The CO₂ reduction reaction is a cathodic reaction. If the metal oxide is used as the electrocatalyst for CO₂ reduction, it will be reduced first on the cathode [24]. The nano-sized metals synthesized by reduction of the metal oxide precursors were found to catalyze the reduction of CO₂ efficiently [2, 21, 25, 26]. In this work, the nano-sized Bi₂O₃ and its precursor (without calcination) were synthesized and in situ reduced to the metal Bi separately on the glass carbon electrodes. The two kinds of metal Bi were used as the electrocatalysts for the reduction of CO₂, and their catalytic performances (such as selectivity, reaction rate and stability) were investigated and compared.

2. EXPERIMENTAL

2.1 Electrode preparation

The Bi₂O₃ was prepared via hydrothermal method. NH₄OH solution was added to 0.1 mol L⁻¹ Bi(NO₃)₃·5H₂O aqueous solution drop by drop until the pH value of the solution reached 8~10 with stirring. Then, the mixed solution was transferred into stainless steel autoclave and heated at 130 °C for 6 h. The obtained white sample was the precursor of Bi₂O₃. After calcination at 500 °C for 2 h, the white precursor was converted to the yellow Bi₂O₃.

20 mg of the as-prepared Bi₂O₃ or its precursor was first dissolved in 500 μL of alcohol. Then 50 μL of 5% Nafion solution was added to the solution. Finally, the sample solution was subjected to sonication treatment. A L-style glass carbon electrode (GCE, 5 mm in diameter) was polished with alumina powder, followed by sonication in alcohol and deionized water successively and dried under nitrogen. Then, 10 μL of the as-prepared sample solution was cast onto the GCE and dried in air. The precursor and Bi₂O₃ modified GCEs were reduced at -1.5 V vs. Ag/AgCl in 0.1 mol L⁻¹ KHCO₃ aqueous solutions for 5 min, respectively. After the reduction processes, the white precursor and the yellow Bi₂O₃ both turned to black. The reductive precursor and Bi₂O₃ were named Re-P and Re-Bi₂O₃, respectively.

2.2 Electrochemical experiments

The electrochemical experiments were performed in an undivided three-electrode glass cell with 20 mL electrolyte. The working electrode was the Re-P modified GCE (Re-P/GCE) or Re-Bi₂O₃

modified GCE (Re-Bi₂O₃/GCE). A Pt plate (2 cm²) and an Ag/AgCl electrode (sat. KCl) were chosen as the counter electrode and the reference electrode, respectively. The electrolyte used was 0.1 mol L⁻¹ KHCO₃ aqueous solution.

Electrochemical measurements were carried out using a CHI 660E electrochemical workstation (Shanghai Chenhua Instruments Co., Ltd., China). Linear sweep voltammetry (LSV) was performed in N₂-saturated or CO₂-saturated electrolyte which was prepared by being bubbled with N₂ or CO₂ for 30 min. The potential scan rate was 0.05 V s⁻¹. The current density is determined on the area of the GCE. Electrochemical impedance spectroscopy (EIS) was performed in CO₂-saturated electrolyte, which was recorded at the frequency range from 5 × 10⁴ to 0.1 Hz with an amplitude of 0.01 V. Controlled potential electrolysis was carried out using a LAND CT2001C cell performance-testing instrument (Wuhan Electronics Co., Ltd., China). The electrolyte was saturated with CO₂ before the electrolysis experiment and was aerated with CO₂ continuously at a flow rate of 10 mL min⁻¹ during the electrolysis process. The total charge passed was 10 C.

2.3 Analysis and calculations

Scanning electron microscope (SEM) images were taken with a Hitachi S-4800 microscope. X-ray diffraction (XRD) patterns were recorded on a Bruker D8 Advance powder X-ray diffractometer using Cu K α radiation (wavelength $\lambda = 0.15406$ nm). The valence state of Bi on the surfaces of the electrocatalysts was quantified by X-ray photoelectron spectroscopy (XPS, ESCALAB 250Xi). Ion chromatography (IC) data was obtained for quantifying the concentration of formate product in the electrolyte using a Dionex ICS-5000⁺ IC instrument.

The faradaic efficiency for producing formate (f) can be determined by equation (1):

$$f = 2nF / Q \quad (1)$$

where n is the number of moles of produced formate which can be calculated according to IC data; F is Faraday's constant (96485 C mol⁻¹); and Q is the total charge passed during the electrolysis ($Q = 10$ C here).

3. RESULTS AND DISCUSSION

For the precursor of Bi₂O₃, its XRD pattern shown in Fig. 1a is differently than that of Bi₂O₃, there is no corresponding standard spectrum in the XRD database. It can be seen from Figs. 2a and b that the precursor shows flower-like morphology which consists of crisscrossed two-dimensional thin sheets with the thickness between 20 and 40 nm. After calcination at 500 °C for 2 h, the precursor became Bi₂O₃. The XRD pattern of the prepared Bi₂O₃ can be seen in Fig. 1b. The characteristic peaks of the prepared Bi₂O₃ can be perfectly indexed as monoclinic Bi₂O₃ (JCPDS cards No. 72-0398). This observation is characteristic of the monoclinic structure of Bi₂O₃ in according with the reported case [27]. As shown in Figs. 2c and d, the prepared Bi₂O₃ has the morphology of anomalous nanosheets and nanoparticles. The precursor being converted to Bi₂O₃ after calcination at 500 °C indicates that the

doped element is volatile. Due to the initial reaction reagents are $\text{Bi}(\text{NO}_3)_3 \cdot 5\text{H}_2\text{O}$ and NH_4OH , therefore, we can propose that the precursor is Bi-based compound containing nitrate or amino.

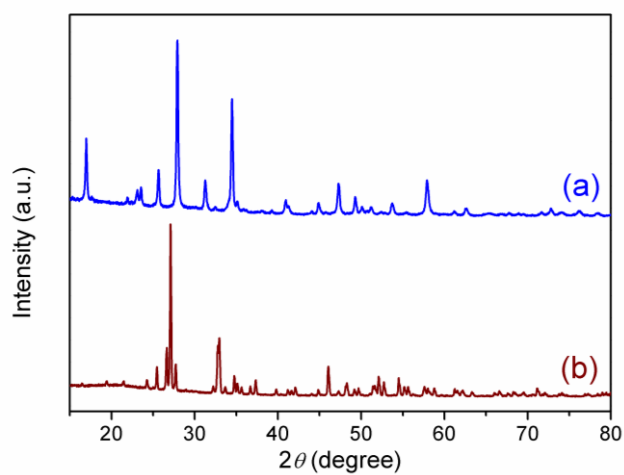


Figure 1. XRD patterns of the precursor (a) and Bi_2O_3 (b).

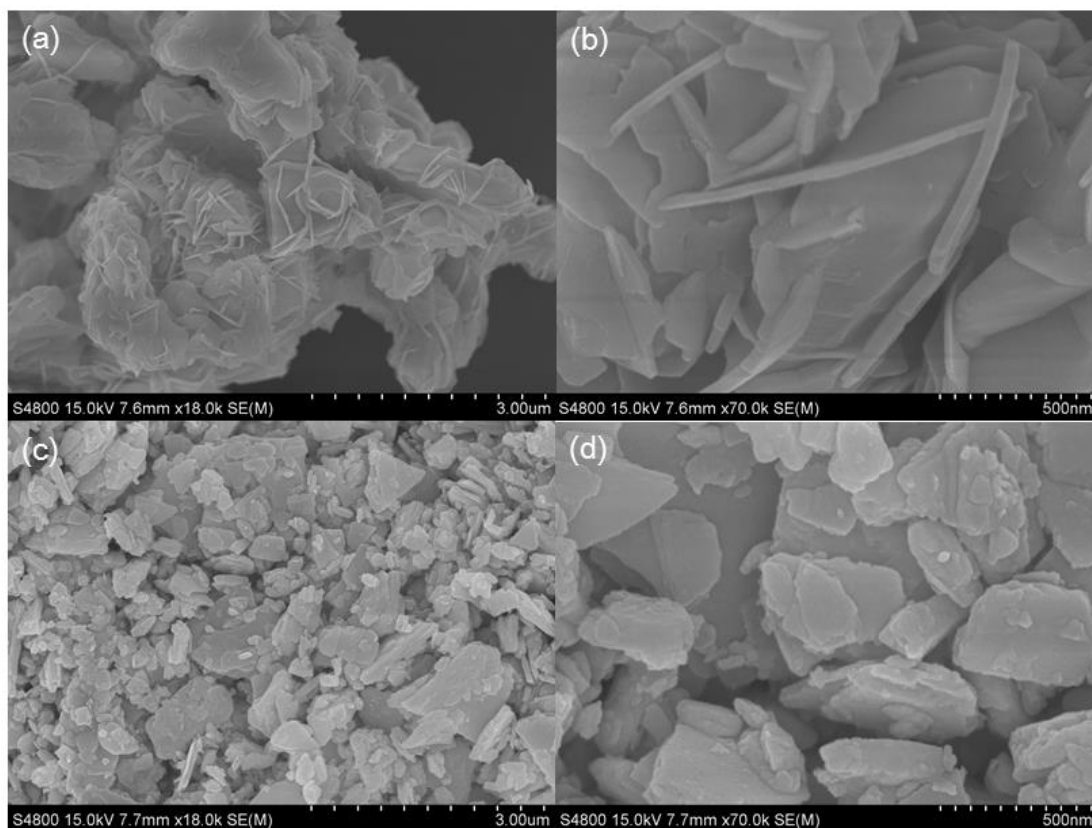


Figure 2. SEM images of the precursor (a, b) and Bi_2O_3 (c, d).

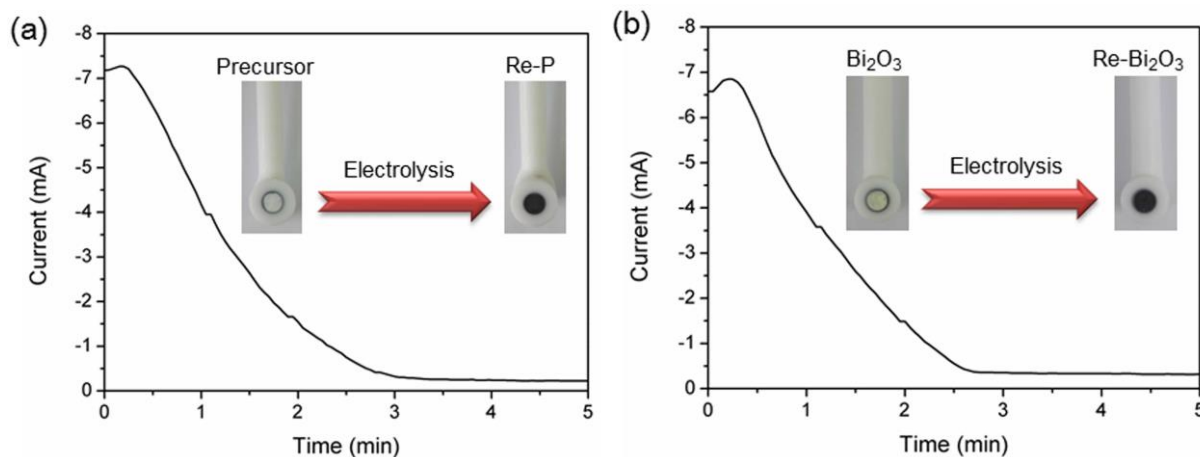
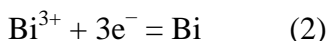


Figure 3. Currents versus time during the electrochemical reduction of the precursor to Re-P (a) or electrochemical reduction of Bi_2O_3 to Re- Bi_2O_3 (b) at -1.5 V for 5 min. The insert images are the photos of the modified GCEs before and after electrochemical reduction.

Zhang et al. reported that nano-sized Bi can be obtained from the electrochemical reduction of BiOCl at the potentials less than -1.16 V vs. SCE [21]. In this paper, the same method was used to reduce the precursor and Bi_2O_3 to metal Bi, respectively. The reduction potential was set at -1.5 V vs. Ag/AgCl . Fig. 3 shows the current-time curves during the electrochemical reduction of the precursor and Bi_2O_3 for 5 min. It can be seen that the colors of the precursor and Bi_2O_3 on the GCEs turn black which is the characteristic color of metal Bi (see the insets of Figs. 3a and b) after the reduction process. The colors of the metal Bi and the oxidized Bi are different, thus we can assume by the color changes that the oxidized Bi in the precursor and Bi_2O_3 have been reduced to metal Bi. The reaction equation is:



The reductive precursor and Bi_2O_3 were named Re-P and Re- Bi_2O_3 , respectively, which were used as the electrocatalysts for the reduction of CO_2 in the following experiments.

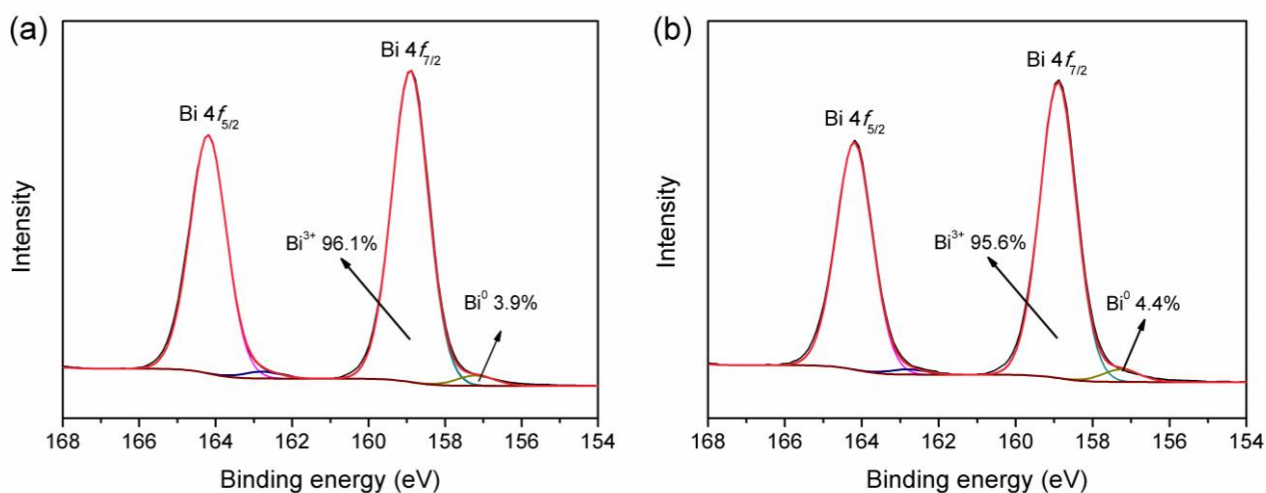


Figure 4. High-resolution XPS spectra recorded for Bi 4f region of the Re-P and Re- Bi_2O_3 .

Determine the structure of the catalyst surface only by the color change is not comprehensive. It was reported that the metastable metal oxides are known to persist on electrode surfaces during cathodic reactions [25, 28, 29]. Furthermore, the metal Bi is readily oxidized in the air [30]. Therefore, we further investigated the surface state of the Re-P and Re-Bi₂O₃ electrocatalysts by XPS. Fig. 4 shows the high-resolution XPS spectra recorded for Bi 4*f* region of Re-P and Re-Bi₂O₃. Bi 4*f*_{7/2} spectra recorded for Re-P and Re-Bi₂O₃ can fit to two components at 158.9 and 157.3 eV those correspond to Bi³⁺ and Bi⁰, respectively [31]. The peak area percentages of Bi³⁺ are 96.1% and 95.6% for Re-P and Re-Bi₂O₃, respectively. Through the analysis of the XPS results, it is realized that the active substance on the surfaces of Re-P and Re-Bi₂O₃ is BiO_x/Bi.

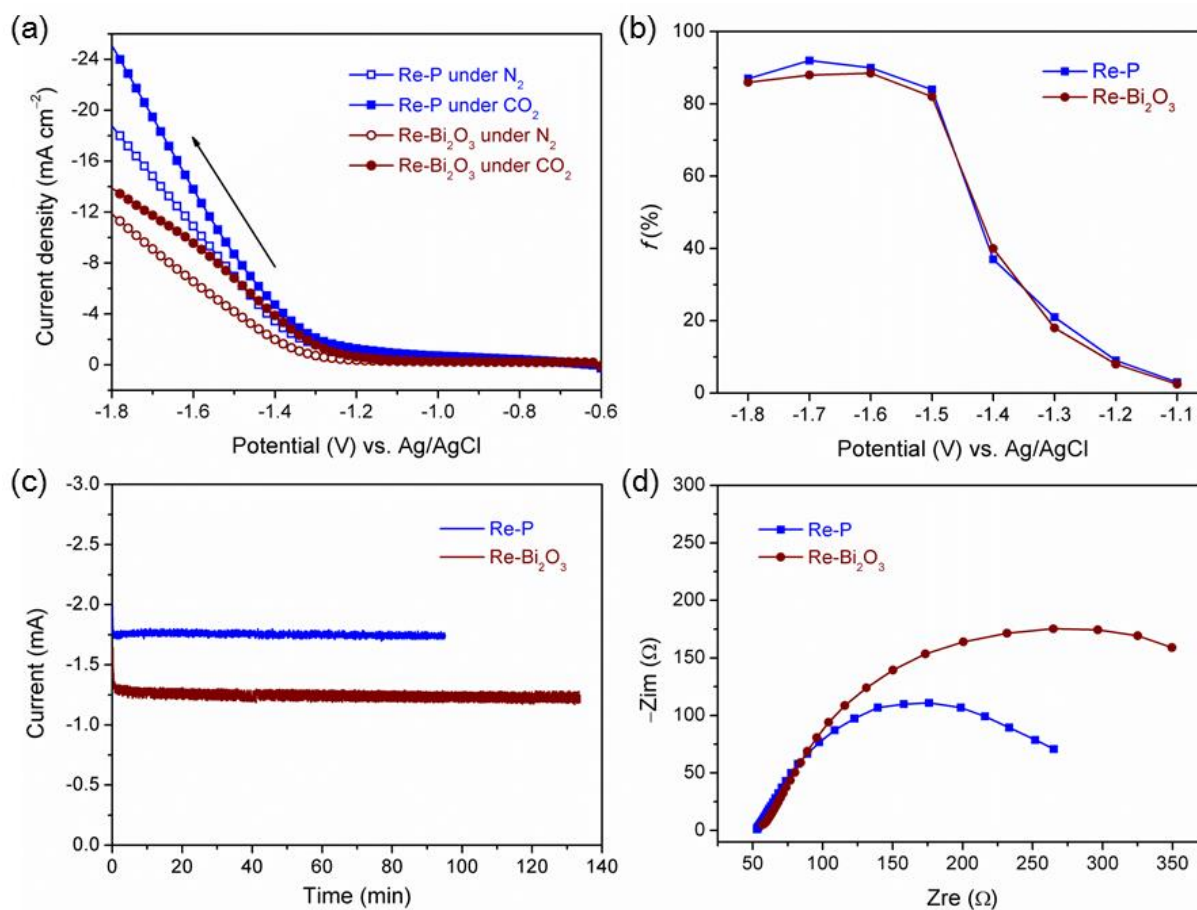


Figure 5. (a) LSV curves obtained on Re-P/GCE and Re-Bi₂O₃/GCE in N₂-saturated (hollow) or CO₂-saturated (solid) 0.1 mol L⁻¹ KHCO₃ solutions. (b) Faradaic efficiencies of Re-P and Re-Bi₂O₃ at various electrolysis potentials; (c) Current-time curves of Re-P and Re-Bi₂O₃ for the reduction of CO₂ at -1.5 V for 10 C. (d) Nyquist plots for the EIS analysis on Re-P/GCE and Re-Bi₂O₃/GCE in CO₂-saturated 0.1 mol L⁻¹ KHCO₃ solutions.

Fig. 5a depicts the LSV curves obtained on Re-P/GCE and Re-Bi₂O₃/GCE in N₂-saturated and CO₂-saturated 0.1 mol L⁻¹ KHCO₃ solutions. On the cathodic end of the CV curves, sharp increases of the current densities can be observed under both N₂ and CO₂. Under N₂, this increase is due to the evolution of H₂ only; under CO₂, the enhanced current must be caused by both the reduction of CO₂ and the evolution of H₂. For Re-P and Re-Bi₂O₃, the current densities under CO₂ are bigger than those

under N₂. At the potential of -1.8 V, the current density of Re-P and Re-Bi₂O₃ are 24.9 and 14.0 mA cm⁻². As we know, high processing temperature leads to high crystallinity of the materials. After calcining the precursor at 500 °C for 2 h, the prepared Bi₂O₃ possesses high crystallinity which may reduce the surface active site. The precursor was not treated by calcination, thus Re-P shows higher current density than Re-Bi₂O₃.

Electrolysis experiments were performed applying a constant potential in the range from -1.1 to -1.8 V at 0.1 V intervals. Fig. 5b shows the faradaic efficiencies for producing formate obtained at various electrolysis potentials. The faradaic efficiencies on Re-P/GCE and Re-Bi₂O₃/GCE both increase as the potential decreases. It can be seen that the difference of the faradaic efficiencies between Re-P and Re-Bi₂O₃ is small, which may related to their similar surface states (Fig. 4).

The overpotential is an important indicator to evaluate the catalytic performance of the electrocatalyst. The overpotential (η) in this work can be calculated by Eq. (3):

$$\eta = E^\circ - E \text{ (vs. Ag/AgCl)} - 0.20 \text{ V} \quad (3)$$

where E° is the standard electrode potential for the reduction of CO₂ to HCOO⁻ ($E^\circ = -0.41$ V vs. SHE at pH 7.0) [8]. We can see that the highest faradaic efficiency obtained in this work is 92% on Re-P/GCE at -1.7 V (the corresponding overpotential is 1.09 V). The faradaic efficiencies for producing formate at -1.5 V on Re-P/GCE and Re-Bi₂O₃/GCE are 84% and 82%, respectively. The corresponding overpotential is 0.89 V, which is lower than those of Sn-based electrocatalysts (1.19 V) in our previous work and is helpful to reduce the energy input of the reaction in industry application [32, 33]. Lower overpotential for the CO₂ reduction reaction is desired in the practical application.

As shown in Table 1, at the electrolysis potential of -1.8 V, the current density of Re-P can achieve to 24.9 mA cm⁻², which is a high value compared to most of the electrocatalysts used for the reduction of CO₂ to formate. At the same electrolysis condition, the current density of Sn plate was only 3.7 mA cm⁻², and those of nanostructured Sn and porous Sn were 10.2 and 7.4 mA cm⁻², respectively. At the potential of -1.5 V, the current density of Re-P can achieve to 9.1 mA cm⁻², which is almost 3 times as big as that of nano-sized Bi electrocatalyst.

Table 1. Comparison of the catalytic performances of Re-P and the similar electrocatalysts reported in literature for the reduction of CO₂ to formate.

Electrocatalyst	Potential (V)	f (%)	Current density (mA cm ⁻²)	Ref.
Sn plate	-1.8 V (vs. Ag/AgCl)	84.0	3.7	[34]
Nanostructured Sn	-1.8 (vs. SCE)	93.6	10.2	[22]
Porous Sn	-1.8 V (vs. Ag/AgCl)	91.5	7.4	[20]
Re-P	-1.8 V (vs. Ag/AgCl)	86.0	24.9	This work
Nano-sized Bi	-1.5 V (vs. Ag/AgCl)	91.3	3.1	[23]
Re-P	-1.5 V (vs. Ag/AgCl)	84.0	9.1	This work

Fig. 5c shows the current-time curves of Re-P and Re-Bi₂O₃ for the reduction of CO₂ at -1.5 V for 10 C. It can be seen that Re-P has larger electrolysis current and shorter electrolysis time than Re-

Bi₂O₃. Re-P has faster reaction rate than Re-Bi₂O₃ with the same passed charge (10 C here). As we known, the reaction rate is an important parameter in the industrial application. If the current density of an electrode is small, in order to complete the production target, large electrode area or long electrolysis time will be required. In contrary, the efficient electrocatalysts with fast reaction rate can save time and implementation costs greatly. Therefore, the Re-P electrocatalyst shows good application prospect for the reduction of CO₂ to formate.

Fig. 5d shows the Nyquist plots obtained on Re-P/GCE and Re-Bi₂O₃/GCE in CO₂-saturated 0.1 mol L⁻¹ KHCO₃ solutions. Since the onset potential for the electrochemical reduction of CO₂ to formate was around -1.3 V (see LSV results in Fig. 5a), the applied potential was set at -1.3 V. It can be seen that the Nyquist plots of Re-P and Re-Bi₂O₃ both show a semicircle. The two semicircles are started at around 50 Ω, which indicates that the values of the solution resistance for Re-P and Re-Bi₂O₃ are similar. The semicircle of Re-P is smaller than that of Re-Bi₂O₃, which means the charge transfer resistance for CO₂ reduction on Re-P is smaller than that on Re-Bi₂O₃. The above results from Fig. 5 indicate that the Re-P electrocatalyst has excellent performance toward CO₂ reduction.

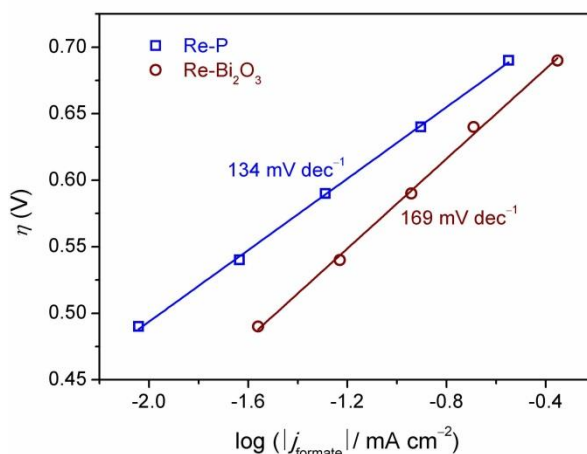


Figure 6. Tafel plots of Re-P and Re-Bi₂O₃ for the electrochemical reduction of CO₂ to formate;

To investigate the mechanism for the reduction of CO₂ to HCOO⁻ on Re-P and Re-Bi₂O₃ electrocatalysts, Tafel plots were extracted, over the overpotential ranging from 0.49 to 0.69 V (Fig. 6). When the Tafel slope is close to 118 mV dec⁻¹, the supported mechanism occurs via a CE mechanism which proceeds through an initial rate-determining transfer of one electron to CO₂; when the Tafel slope is close to 59 mV dec⁻¹, the supported mechanism involves a reversible transfer of one electron to CO₂ to form CO₂^{•-} prior to a chemical rate-determining step [25]. The Tafel slopes of Re-P and Re-Bi₂O₃ for the reduction of CO₂ to HCOO⁻ are 134 and 169 mV dec⁻¹, respectively. These Tafel slopes are close to 118 mV dec⁻¹, which indicates that the reaction occurs via a CE mechanism.

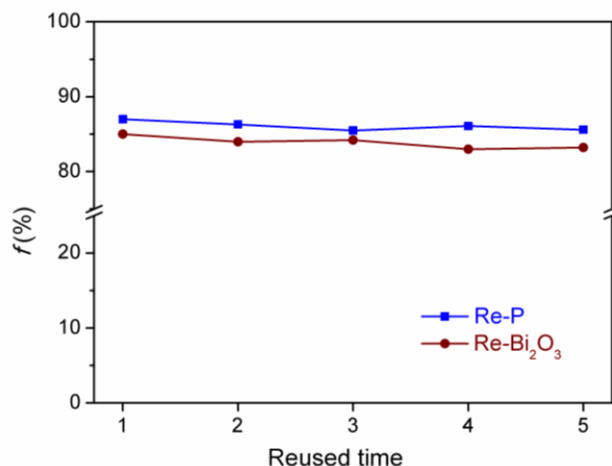


Figure 7. Variations of the faradaic efficiencies for producing formate with the reused time of Re-P/GCE and Re-Bi₂O₃/GCE in electrochemical reduction of CO₂ at -1.5 V.

The stability is an important indicator for assessing the performance of an electrocatalyst. Therefore, we carried out the experiments for investigating the stability of Re-P/GCE and Re-Bi₂O₃/GCE. The electrodes were used to reduce CO₂ electrochemically for 10 C each time, then the electrolyte solution was analyzed for the faradaic efficiency, and then the solution was renewed and did the same thing for 5 times, the results are shown in Fig. 7. It is not obvious that the faradaic efficiency is influenced by such reusing. Therefore, Re-P/GCE and Re-Bi₂O₃/GCE are stable for long term use.

4. CONCLUSIONS

In this paper, flow-like nano-sized Bi₂O₃ precursor was prepared by the method of hydrothermal synthesis. After calcination at 500 °C for 2 h, the precursor was converted to pure Bi₂O₃, but the morphology was broken to irregularly shape. Re-P and Re-Bi₂O₃ were obtained by reduction of the precursor and Bi₂O₃ on the modified GCEs, respectively. The faradaic efficiencies for the electrochemical reduction of CO₂ to formate on Re-P/GCE and Re-Bi₂O₃/GCE were 85% and 82% at an overpotential of 0.89 V, respectively. The faradaic efficiencies did not obviously changed after Re-P/GCE and Re-Bi₂O₃/GCE were reused for five 10 C electrolytic processes. The faradaic efficiencies between Re-P and Re-Bi₂O₃ were not significantly different, whereas the current density of Re-P is larger than that of Re-Bi₂O₃ obviously. It indicates that Re-P is an efficient electrocatalyst for the reduction of CO₂ to formate with high efficiency and stability.

ACKNOWLEDGEMENT

The work was supported by the National Natural Science Foundation of China (grant numbers 21603184, 21575123); and the joint research fund between Collaborative Innovation Center for

Ecological Building Materials and Environmental Protection Equipments and Key Laboratory for Advanced Technology in Environmental Protection of Jiangsu Province.

References

1. J. L. Qiao, Y. Y. Liu, F. Hong, J. J. Zhang, *Chem. Soc. Rev.*, 43 (2014) 631-675.
2. C. W. Li, M. W. Kanan, *J. Am. Chem. Soc.*, 134 (2012) 7231-7234.
3. S. Gao, Y. Lin, X. C. Jiao, Y. F. Sun, Q. Q. Luo, W. H. Zhang, D. Q. Li, J. L. Yang, Y. Xie, *Nature*, 529 (2016) 68-71.
4. I. Ganesh, *Renew. Sust. Energ. Rev.*, 59 (2016) 1269-1297.
5. T. Vo, K. Purohit, C. Nguyen, B. Biggs, S. Mayoral, J. L. Haan, *ChemSusChem*, 8 (2015) 3853-3858.
6. P. Kang, Z. Chen, A. Nayak, S. Zhang, T. J. Meyer, *Energ. Environ. Sci.*, 7 (2014) 4007-4012.
7. S. Aoi, K. Mase, K. Ohkubo, S. Fukuzumi, *Chem. Commun.*, 51 (2015) 10226-10228.
8. X. Q. Min, M. W. Kanan, *J. Am. Chem. Soc.*, 137 (2015) 4701-4708.
9. Z. M. Detweiler, J. L. White, S. L. Bernasek, A. B. Bocarsly, *Langmuir*, 30 (2014) 7593-7600.
10. T. Sekimoto, M. Deguchi, S. Yotsuhashi, Y. Yamada, T. Masui, A. Kuramata, S. Yamakoshi, *Electrochem. Commun.*, 43 (2014) 95-97.
11. Y. Lan, S. Ma, J. Lu, P. J. A. Kenis, *Int. J. Electrochem. Sci.*, 9 (2014) 7300-7308.
12. S. Zhang, P. Kang, S. Ubnoske, M. K. Brennaman, N. Song, R.L. House, J.T. Glass, T.J. Meyer, *J. Am. Chem. Soc.*, 136 (2014) 7845-7848.
13. R. Kortlever, I. Peters, S. Koper, M. T. M. Koper, *ACS Catal.*, 5 (2015) 3916-3923.
14. X. Y. Zhao, B. B. Luo, R. Long, C. M. Wang, Y. J. Xiong, *J. Mater. Chem. A*, 3 (2015) 4134-4138.
15. G. K. S. Prakash, F. A. Viva, G. A. Olah, *J. Power Sources*, 223 (2013) 68-73.
16. R. Zhang, W. X. Lv, G. H. Li, M. A. Mezaal, L. X. Lei, *RSC Adv.*, 5 (2015) 68662-68667.
17. R. Zhang, W. X. Lv, G. H. Li, M. A. Mezaal, X. J. Li, L. X. Lei, *J. Power Sources*, 272 (2014) 303-310.
18. W. X. Lv, R. Zhang, P. R. Gao, L. X. Lei, *J. Power Sources*, 253 (2014) 276-281.
19. W. X. Lv, J. Zhou, J. J. Bei, R. Zhang, F. Y. Kong, W. Wang, *Int. J. Electrochem. Sci.*, 11 (2016) 6183-6191.
20. W. X. Lv, J. Zhou, F. Y. Kong, H. L. Fang, W. Wang, *Int. J. Hydrogen Energ.*, 41 (2016) 1585-1591.
21. H. Zhang, Y. Ma, F. J. Quan, J. J. Huang, F. L. Jia, L. Z. Zhang, *Electrochem. Commun.*, 46 (2014) 63-66.
22. S. Zhang, P. Kang, T. J. Meyer, *J. Am. Chem. Soc.*, 136 (2014) 1734-1737.
23. W. X. Lv, J. Zhou, J. J. Bei, R. Zhang, L. Wang, Q. Xu, W. Wang, *Appl. Surf. Sci.*, 393 (2017) 191-196.
24. R. Zhang, W. X. Lv, G. H. Li, L. X. Lei, *Mater. Lett.*, 141 (2015) 63-66.
25. Y. H. Chen, M.W. Kanan, *J. Am. Chem. Soc.*, 134 (2012) 1986-1989.
26. Y. H. Chen, C. W. Li, M. W. Kanan, *J. Am. Chem. Soc.*, 134 (2012) 19969-19972.
27. L. W. Shan, G. L. Wang, L. Z. Liu, Z. Wu, *J. Mol. Catal. A-Chem.*, 406 (2015) 145-151.
28. D. Rochefort, P. Dabo, D. Guay, P. M. A. Sherwood, *Electrochim. Acta*, 48 (2003) 4245-4252.
29. M. F. Baruch, J. E. Pander, J. L. White, A. B. Bocarsly, *ACS Catal.*, 5 (2015) 3148-3156.
30. Z. Y. Zhang, X. F. Cui, G. M. Veith, P. F. Zhang, D. A. Lutterman, J. Rosenthal, S. H. Overbury, S. Dai, and H. Y. Zhu, *ACS Catal.*, 6 (2016) 6255- 6264.
31. J. Medina-Ramos, R. C. Pupillo, T.P. Keane, J. L. DiMeglio, J. Rosenthal, *J. Am. Chem. Soc.*, 137 (2015) 5021-5027.
32. D. T. Whipple, P. J. A. Kenis, *J. Phys. Chem. Lett.*, 1 (2010) 3451-3458.
33. B. A. Rosen, A. Salehi-Khojin, M. R. Thorson, W. Zhu, D. T. Whipple, P. J. A. Kenis, R. I. Masel, *Science*, 334 (2011) 643-644.

34. R. Zhang, W. X. Lv, L. X. Lei, *Appl. Surf. Sci.*, 356 (2015) 24-29.

© 2017 The Authors. Published by ESG (www.electrochemsci.org). This article is an open access article distributed under the terms and conditions of the Creative Commons Attribution license (<http://creativecommons.org/licenses/by/4.0/>).